

Inferring the effective start dates of non-pharmaceutical interventions during COVID-19 outbreaks

Ilia Kohanovski¹, Uri Obolski^{2,3}, and Yoav Ram^{1,4,a}

¹School of Computer Science, Interdisciplinary Center Herzliya, Herzliya 4610101, Israel

²School of Public Health, Tel Aviv University, Tel Aviv 6997801, Israel

³Porter School of the Environment and Earth Sciences, Tel Aviv University, Tel Aviv 6997801, Israel

⁴School of Zoology, Faculty of Life Sciences, Tel Aviv University, Tel Aviv 6997801, Israel

^aCorresponding author: yoav@yoavram.com, ORCID 0000-0002-9653-4458

January 21, 2021

Abstract

During Feb-Apr 2020, many countries implemented non-pharmaceutical interventions, such as school closures and lockdowns, with variable schedules, to control the COVID-19 pandemic caused by the SARS-CoV-2 virus. Overall, these interventions seem to have reduced the spread of the pandemic. We hypothesize that the official and effective start date of such interventions can be noticeably different, for example due to slow adoption by the population, or because the authorities and the public are unprepared. We fit an SEIR model to case data from 12 regions to infer the effective start dates of interventions and contrast them with the official dates. We find mostly late, but also early effects of interventions. For example, Italy implemented a nationwide lockdown on Mar 11, but we infer the effective date on Mar 17 ($^{+3.05}_{-2.01}$ days 95% CI). In contrast, Germany announced a lockdown on Mar 22, but we infer an effective start date on Mar 19 ($^{+0.92}_{-0.99}$ days 95% CI). We demonstrate that differences between the official and effective start of NPIs can lead to under-estimating their impact, and discuss potential causes and consequences of our results.

Keywords: SEIR, COVID-19, public health, epidemic, infectious disease, NPI

Introduction

26 The COVID-19 pandemic has resulted in implementation of extreme non-pharmaceutical interventions
27 (NPIs) in many affected countries. These interventions, from social distancing to lockdowns, are
28 applied in a rapid and widespread fashion. NPIs are designed and assessed using epidemiological
29 models, which follow the dynamics of infection to forecast the effect of different mitigation and
30 suppression strategies on the levels of infection, hospitalization, and fatality. These epidemiological
31 models usually assume that the effect of NPIs on infection dynamics begins at the officially declared
32 date^{9,11,17}.

33 Adoption of public-health recommendations is often critical for effective response to infectious dis-
34 eases, and has been studied in the context of HIV¹⁵ and vaccination^{6,22}, for example. However,
35 behavioural and social change does not occur immediately, but rather requires time to diffuse in the
36 population through media, social networks, and social interactions. Moreover, compliance to NPIs
37 may differ between different interventions and between people with different backgrounds. For ex-
38 ample, in a survey of 2,108 adults in the UK during Mar 2020, Atchison et al.³ found that those over
39 70 years old were more likely to adopt social distancing than young adults (18-34 years old), and that
40 those with lower income were less likely to be able to work from home and to self-isolate. Similarly,
41 compliance to NPIs may be impacted by personal experiences. Smith et al.¹⁹ have surveyed 6,149
42 UK adults in late Apr 2020 and found that people who believe they have already had COVID-19 are
43 more likely to think they are immune, and less likely to comply with social distancing guidelines.
44 Compliance may also depend on risk perception as perceived by the the number of domestic cases or
45 even by reported cases in other regions and countries. Interestingly, the perceived risk of COVID-19
46 infection has likely caused a reduction in the number of influenza-like illness cases in the US starting
from mid-Feb 2020²³.

47 Here, we hypothesise that there is a significant difference between the official start of NPIs and their
48 effective adoption by the public and therefore their effect on infection dynamics. We use a *Susceptible-*
49 *Exposed-Infected-Recovered* (SEIR) model and a *Markov Chain Monte Carlo* (MCMC) parameter
50 estimation framework to infer the effective start date of NPIs from publicly available COVID-19 case
51 data in 12 geographical regions. We compare these estimates to the official dates, and find that they

Country	First	Last
Austria	Mar 10 2020	Mar 16 2020
Belgium	Mar 12 2020	Mar 18 2020
Denmark	Mar 12 2020	Mar 18 2020
France	Mar 13 2020	Mar 17 2020
Germany	Mar 12 2020	Mar 22 2020
Italy	Mar 5 2020	Mar 11 2020
Norway	Mar 12 2020	Mar 24 2020
Spain	Mar 9 2020	Mar 14 2020
Sweden	Mar 12 2020	Mar 18 2020
Switzerland	Mar 13 2020	Mar 20 2020
United Kingdom	Mar 16 2020	Mar 24 2020
Wuhan	Jan 23 2020	Jan 23 2020

Table 1: Official start of non-pharmaceutical interventions. The date of the first intervention is for a ban of public events, or encouragement of social distancing, or for school closures. In all countries except Sweden, the date of the last intervention (τ^*) is for a lockdown. In Sweden, where a lockdown was not ordered during the studied dates, the last date is for school closures. Dates for European countries from Flaxman et al.⁹, date for Wuhan, China from Pei and Shaman¹⁸. See Figure S1 for a visual presentation.

include both late and early effects of NPIs on infection dynamics. We conclude by demonstrating
54 how differences between the official and effective start of NPIs can confound assessments of their
impacts.

56 Results

Several studies have described the effects of non-pharmaceutical interventions in different geographical
58 regions^{9,11,17}. Some of these studies have assumed that the parameters of the epidemiological model
change at a specific date (Eq. 6), and set the change date τ to the official NPI date τ^* , usually the
60 lockdown start date (Table 1). They then fit the model once for time $t < \tau^*$ and once for time $t \geq \tau^*$.
For example, Li et al.¹⁷ estimate the infection dynamics in China before and after τ^* , which is set at
62 Jan 23, 2020. Thereby, they effectively estimate the transmission and reporting rates before and after
 τ^* separately.

64 Here, we estimate the joint posterior distribution of the effective start date of NPIs, τ , and the
transmission and reporting rates before and after τ from the entire data, rather than splitting the data
66 at τ . This is done under the simplifying assumption that all interventions start at a specific date, despite
the reality that the durations between the first and last NPIs were between 4 and 12 days (Table 1,
68 Figure S1). We then estimate $\hat{\tau}$ as the median of the marginal posterior distribution of τ . Credible

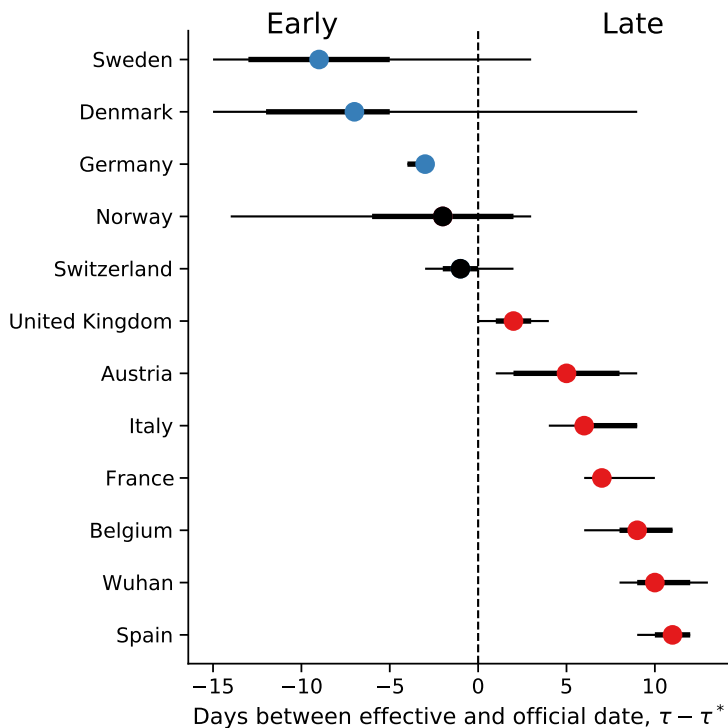


Figure 1: Official vs. effective start of non-pharmaceutical interventions. The difference between τ the effective and τ^* the official start of NPIs is shown for different regions. The effective date is delayed in UK, Austria, Italy, France, Belgium, Spain, and Wuhan, China, compared to the official date (red markers). In contrast, the estimated effective dates in Sweden, Denmark, and Germany are earlier than the official dates (blue markers), although uncertainty is low only for Germany (i.e., zero is not in 95% CI). The credible intervals for Sweden, Denmark, and Norway are especially wide, see text and Figure 3 for possible explanation. Here, the markers show $\hat{\tau}$, the marginal posterior median (Table 2). τ^* is the last NPI date (a lockdown, except in Sweden; Table 1). Thin and bold lines show 95% and 75% credible intervals, respectively. Figure S2 shows a similar summary when estimating $\hat{\tau}$ using case data up to Mar 28 rather than Apr 11.

intervals (CI) are calculated as the highest density intervals¹⁶, and their upper and lower boundaries
70 are reported as ${}^{+upper}_{-lower}$ in days relative to $\hat{\tau}$.

We compare the posterior predictive plots of a model with a free τ with those of a model with τ fixed
72 at τ^* and a model without τ (i.e. transmission and reporting rates are constant). All three models
74 were fitted to case data up to Apr 11, used to predict out-of-sample case data up to Apr 24, and these
76 predictions were then compared to the real case data. The model with free τ clearly produces better
78 and less variable predictions (Figure S3): In all 11 of the European countries, the expected posterior
80 RMSE (root mean squared error) of the out-of-sample predictions is lowest for the model with a free τ
82 (Table S2). When we compare the models using WAIC (Eq. 10), the model with a free τ is strongly
84 preferred in 9 out of 12 countries, the exceptions being Norway (only slight preference), Sweden, and
86 Denmark (Table S1). Indeed, when examining the joint posterior distribution of τ and λ (the latter is
the reduction in transmission due to NPIs, see Eq. 1), high values of λ are estimated in Denmark and
Sweden (0.7 and 0.74, respectively; see Table 2), probably making the inference of τ more difficult
due to unidentifiability, resulting in a wide posterior for τ . Some correlation between the parameters is
also evident in Norway, where λ estimates are low (0.31). Notably, the data for Sweden and Denmark
do not have a single "peak" during the evaluated dates, possibly leading to wide 95% credible intervals
on $\hat{\tau}$ (Figure 1) and poor WAIC in the model with free τ , whereas the duration between the first and
last interventions was especially long in Norway (Table 1).

We compare the official τ^* and effective τ start of NPIs and find that in most regions the effective start
88 of NPIs differs from the official date: in 10 of 12 countries the 75% credible interval on τ does not
90 include τ^* (7 of 12 countries when considering a 95% interval; Figure 1). The exceptions are Norway
and Switzerland (see below). The former also has a wide 95% credible interval, perhaps because it
has the longest duration between the first and last NPIs (Table 1).

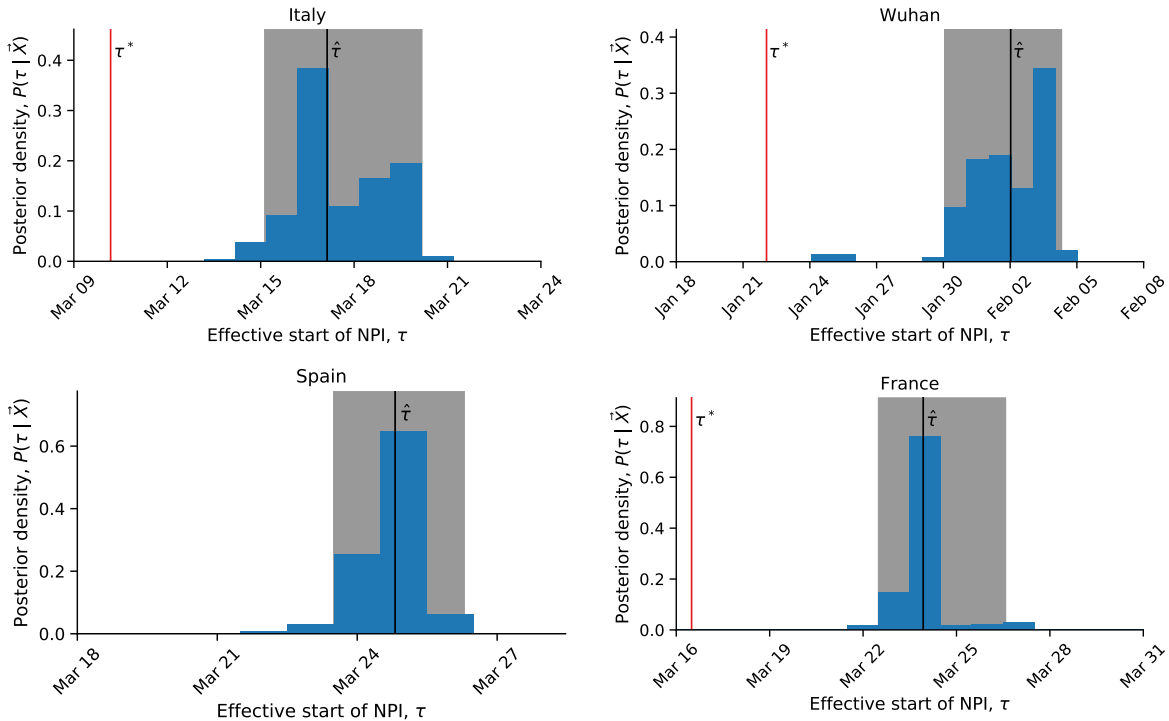


Figure 2: Late effect of non-pharmaceutical interventions. Posterior distribution of τ , the effective start date of NPI, is shown as a histogram of MCMC samples. Red line shows the official last NPI date τ^* . Black line shows the estimated effective start date $\hat{\tau}$. Shaded area shows a 95% credible interval.

92 **Late effective start of NPIs.** In half of the examined regions, we estimate that the effective start of NPIs τ is later than the official date τ^* .

94 In Italy, the first case was officially confirmed on Feb 21. School closures were implemented on Mar 5⁹, a lockdown was declared in Northern Italy on Mar 8, with social distancing implemented in
96 the rest of the country, and the lockdown was extended to the entire nation on Mar 11¹¹. That is, the
98 first and last official NPI dates are Mar 5 and Mar 11. However, we estimate the effective date $\hat{\tau}$ six days after the lockdown, at Mar 17 ($^{+3.05}_{-2.01}$ days 95% CI; Figure 2).

In Wuhan, China, a lockdown was ordered on Jan 23¹⁷, but we estimate the effective start of NPIs
100 to be ten days later, at Feb 2 ($^{+2.29}_{-2.97}$ days 95% CI), although there is low but noticeable posterior
102 probability for Jan 24-25 (Figure 2). Higher estimates of τ (Jan 4) correspond to a wide posterior for
 λ (Figure S4).

In Spain, social distancing was encouraged starting on Mar 8⁹, but mass gatherings still occurred on
104 Mar 8, including a march of 120,000 people for the [International Women's Day](#), and a football match
between [Real Betis](#) and [Real Madrid](#) (final score 2–1) with a crowd of 50,965 in Seville. A national
106 lockdown was only announced on Mar 14⁹. Nevertheless, we estimate the effective start of NPI $\hat{\tau}$
eleven days later, at Mar 25 ($^{+1.70}_{-1.43}$ days 95 %CI, Figure 2).

108 Similarly, in France we estimate the effective start of NPIs $\hat{\tau}$ at Mar 24 ($^{+2.65}_{-1.44}$ days 95% CI, Figure 2).
This is a week later than the official lockdown, which started at Mar 17, and more than 10 days after
110 the earliest NPI, banning of public events, which started on Mar 13⁹.

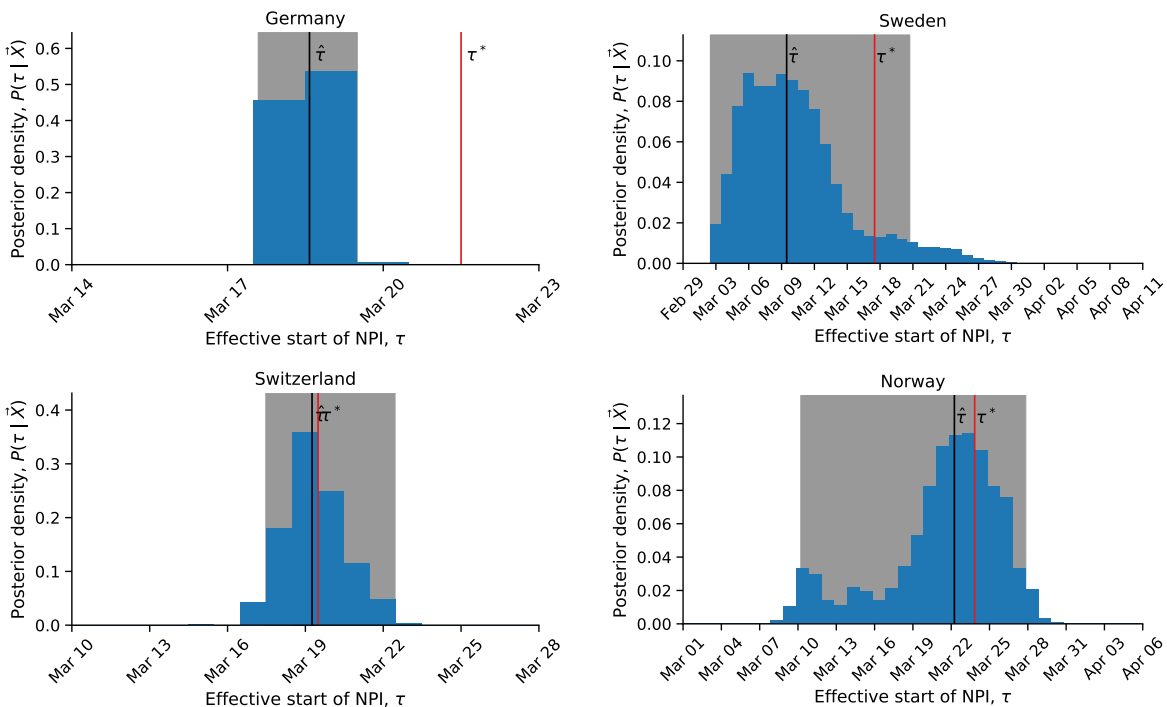


Figure 3: Early and exact effect of non-pharmaceutical interventions. Posterior distribution of τ , the effective start date of NPI, is shown as a histogram of MCMC samples. Red line shows the official last NPI date τ^* . Black line shows the estimated effective start date $\hat{\tau}$. Shaded area shows a 95% credible interval.

112 **Early effective start of NPIs.** In some regions we estimate an effective start of NPIs τ that is *earlier*
then the official date τ^* (Figure 1). The only conclusive early case is Germany, in which we estimate
114 the effective start of NPIs at Mar 19 ($^{+0.92}_{-0.99}$ days 95 %CI; Figure 3). This estimate falls between the
first and last official NPI dates, Mar 12 and Mar 22 (Table 1). Therefore, when we refer to this case as

"early", we mean that the effective date (Mar 19) occurs *before* the official lockdown date (Mar 22),
116 not that it occurs before all NPIs. Interestingly, Germany has the second longest duration between first
and last NPIs after Norway (10 and 12 days respectively; Table 1). However, the credible interval for
118 the effective date in Germany is narrow (1.91 days), whereas it is very wide in Norway (17.61 days).
That τ is significantly earlier than τ^* can suggest that early NPIs in Germany more effectively reduced
120 transmission rates compared to other countries. Another possible interpretation is that the German
population anticipated the lockdown and began to act accordingly before it started.

122 We also estimate an early effective start of NPIs in Denmark, Norway, and Sweden. However, the
credible intervals are quite wide (Figure 1), and in Denmark and Sweden the evidence did not support
124 the model with free τ over the model with τ fixed at the official date (WAIC values in Table S1).
Indeed, Denmark and Sweden had the highest estimates of λ , that is, the smallest estimated effect
126 of NPIs on transmission rates, which probably hinders our ability to estimate τ in these countries
(see also joint posterior distributions in Figure S4). Moreover, in Sweden the number of daily cases
128 continues to grow up to Apr 11, rather than "peak" (Figure S3). In Denmark, the opposite occurs:
there are seemingly two "peaks", on Mar 11 and on Apr 8 (Figure S3); the first "peak" may be a result
130 of stochastic events, for example due to a large cluster of cases or an accumulation of tests. We suspect
that these missing and additional "peaks" increase the uncertainty in our inference.

132 The estimated effective date in Norway is Mar 22, two days earlier than the official date of Mar 24.
However, the posterior distribution is very wide ($^{+5.59}_{-12.03}$ days 95% CI): it covers the range between
134 Mar 10, two days before the first NPI, and Mar 27, three days after the last NPI (Table 1, Figure S1).
The uncertainty in the estimate of the effective start of NPIs might be due to the long duration
136 between the first and last NPIs; however, Germany had the second longest duration between first and
last NPIs, but the corresponding posterior distribution is very narrow (Figure 3). There may also
138 be an unidentifiability issue, as there is some negative correlation between the estimates of τ and λ
(Figure S4).

140 **Exact effective start of NPIs.** We find one case in which the official and effective dates match and
the credible interval is narrow. Switzerland ordered a national lockdown on Mar 20, after banning
142 public events and closing schools on Mar 13 and 14⁹. Indeed, the posterior median $\hat{\tau}$ is Mar 19
($^{+3.2}_{-1.78}$ days 95% CI, see Figure 3). It's also worth mentioning that Switzerland was the first to mandate
144 self isolation of confirmed cases⁹.

146 **Assessment of impact of NPIs.** The *effective reproduction number* R is the average number of
secondary cases caused by an infected individual after an epidemic is already underway⁵. We infer
148 model-based effective reproduction numbers before and after the implementation of NPIs from model
parameters (Eq. 7). We then estimate the impact of NPIs as the relative reduction in the reproduction
number⁹. We compare the impacts estimated using the fixed τ model and the free τ model. That is,
150 we compare the impact estimate assuming that NPIs started at the official date τ^* , versus the estimate
when inferring the effective start of NPIs from the data. Figure 4 demonstrates that estimates from the
152 fixed τ model (y-axis) are consistently lower than estimates from the free τ model (x-axis), except in
Sweden and Denmark, in which estimation uncertainty is high. These results suggest that the impact
154 of past NPIs is likely to be under-estimated by health officials and researchers if they assume NPIs
effectively start at their official dates. The estimated impact can then be interpreted as ineffectiveness
156 of the NPIs, leading to more aggressive NPIs being applied.

158 Health officials might also assess the impact of NPIs by comparing model expectations to actual
number of daily cases at a specific number of days after the intervention began. However, a significant
difference between the official and effective start of interventions can invalidate such assessments.

- 160 This is illustrated in Figure 5 using data and parameters from Italy: a lockdown was officially ordered
 162 on Mar 10 (τ^*), but its late effect on the infection dynamics starts on Mar 17 ($\hat{\tau}$). If health officials
 164 assume that the dynamics change exactly at τ^* , they would expect the number of cases to be within the
 166 red lines (posterior predictions assuming $\tau = \tau^*$). This would lead to a significant under-estimation,
 which might be interpreted as ineffectiveness of NPIs, and therefore more strict guidelines. However,
 the number of cases would actually follow the blue lines (posterior predictions using $\tau = \hat{\tau}$), which
 are a good fit to the real data (stars).

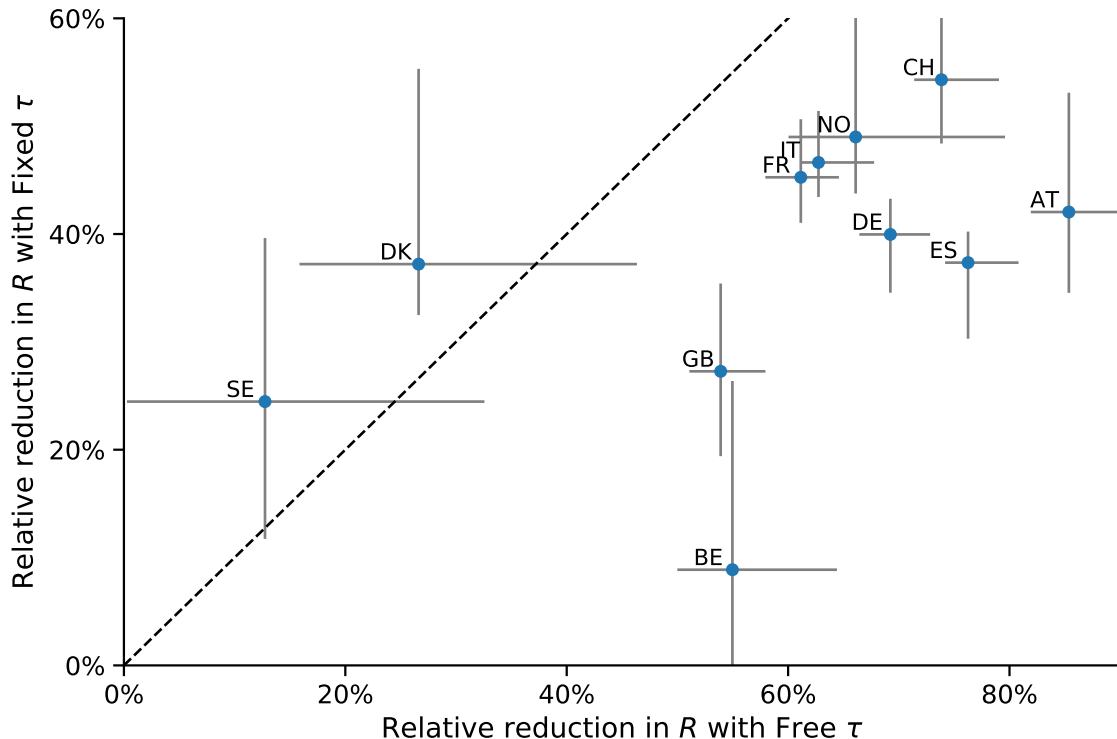


Figure 4: Impact of NPIs is under-estimated when assuming they start at the official date. Shown are estimates of the relative reductions in R (the effective reproduction number), which measures the impact of NPIs on disease transmission, in 11 European countries. The y-axis shows estimates when assuming the start of NPIs is fixed at the official date (fixed τ); the x-axis shows estimates when inferring the effective start of NPIs from the data (free τ). The dashed line shows a one-to-one correspondence. Markers and bars denote the posterior median and 50% credible intervals (HDI). The relative reductions in R are consistently lower for the fixed τ model (below the dashed line), except in Sweden and Denmark in which uncertainty is high.

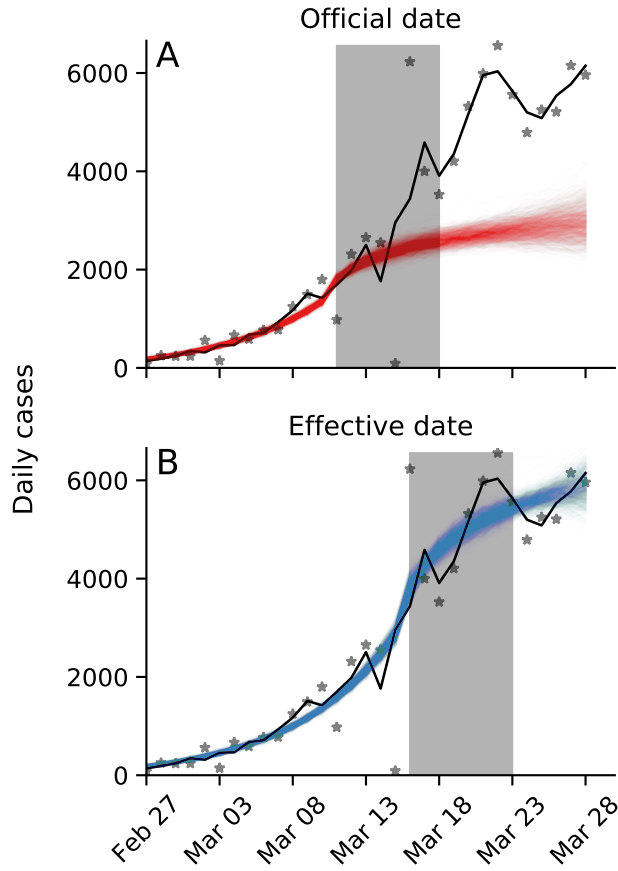


Figure 5: Late effective start of NPIs leads to under-estimation of daily confirmed cases. Real number of daily cases in Italy in black (markers: data; line: smoothed using a Savitzky-Golay filter with window length 3). Model posterior predictions are shown as coloured lines (1,000 draws from the posterior distribution). Shaded box illustrates a serial interval of seven days¹ after the start of NPIs. **(A)** Using the official date τ^* for the effective start of the NPI, Mar 11, the model under-estimates the number of cases seven days after the start of the NPI. **(B)** Using the estimated date $\hat{\tau}$ for the effective start of the NPI, Mar 17, the model precisely estimates the number of cases seven days after the start of the NPI. Here, model parameters are best estimates for Italy (Table 2).

Discussion

168 We have inferred the effective start date of NPIs in several geographical regions using an SEIR model
 169 under an MCMC parameter estimation framework. We find examples of both late and early effective
 170 start of NPIs relative to the official date (Figure 1).

172 In most investigated regions we find late effective start of NPIs. For example, in Italy and in Wuhan,
 173 China, the effective start of the lockdowns seems to have occurred five or more days after the official
 174 date (Figure 2). This difference might be explained, in some cases, by low compliance or non-
 175 adherence to guidelines: In Italy, for example, the government plan to implement a lockdown in
 176 the Northern provinces leaked to the public, resulting in people leaving these provinces before the
 177 lockdown started¹¹. Late effect of NPIs may also be due to the time required by both the government
 178 and the citizens to prepare for a lockdown, and for new guidelines to be adopted by the population.

179 In contrast, in some regions we inferred reduced transmission rates even before official lockdowns
 180 were implemented, although this is only conclusive in Germany (Figure 3). An early effective date
 181 might be due to early adoption of social distancing and similar behavioural adaptations in parts of
 182 the population, possibly due to earlier NPIs or NPIs being applied in other regions. Adoption of

182 these behaviours may occur via media and social networks, rather than official guidelines, and may be
184 influenced by increased risk perception due to domestic or international COVID-19 reports². Indeed,
the evidence supports a change in infection dynamics (i.e. a model with fixed or free τ) even for
Sweden (Table S1, Table S2, Figure S3), where a lockdown was not implemented*.

186 As expected, we have found that the evidence supports a model in which the transmission rate changes
at a specific time point over a model with a constant transmission rate (Tables S1 and S2). It may be
188 interesting to check if the evidence supports a model with *two* or more change-points, rather than one.
Multiple change-points could reflect escalating NPIs (e.g. school closures followed by lockdowns),
190 or an intervention followed by a relaxation. However, interpretation of such models will be harder,
as multiple change-points are also likely to result in parameter unidentifiability, for example due to
192 simultaneous implementations of NPIs⁹.

194 Interestingly, the effective start of NPIs in France and Spain is estimated to have started on Mar 24
and 25, respectively, although the official NPI dates differ significantly: the first NPI in France is only
one day before the last NPI in Spain. The number of daily cases was similar in both countries until
196 Mar 8, but diverged by Mar 13, reaching much higher numbers in Spain (Figure S5). This may suggest
correlations between effective starts of NPIs due to global or international events.

198 As different countries experiment with various intervention strategies, we expect similar shifts to
occur: in some cases the population will be late to comply with new guidelines, whereas in other cases
200 the population will adopt either restrictions or relaxations even before they are formally announced.
Attempts to assess the impact of NPIs^{4,9} generally assume they start at their official date, and that a
202 significant change in the dynamics can be observed roughly seven days after the start of NPIs (due to
the characteristic serial interval of COVID-19¹). However, late and early effective start of NPIs, such
204 as we have inferred, can bias these assessments and lead to wrong conclusions about the impact of
NPIs (Figures 4 and 5).

206 Our results highlight the complex interaction between personal, regional, and global determinants of
behavioral response to an epidemic. Therefore, we emphasize the need to further study heterogeneity
208 in compliance and behavior over both time and space. This can be accomplished both by surveying
differences in compliance within and between populations³, and by incorporating specific behavioral
210 models into epidemiological models^{2,7,21}.

Models and Methods

212 **Data.** We use daily confirmed case data $\mathbf{X} = (X_1, \dots, X_T)$ from 12 regions during Jan–Apr 2020. These
incidence data summarise the number of individuals X_t tested positive for SARS-CoV-2 (using RT-qPCR tests)
214 on each day t . Data for Wuhan, China, from Jan 10 to Feb 8, retrieved from Pei and Shaman¹⁸. Data for
11 European countries, from Feb 20 to Apr 24, retrieved from Flaxman et al.⁹. Where there were multiple
216 sequences of days with zero confirmed cases (e.g. France), we cropped the data to begin with the last sequence
so that our analysis focuses on the first sustained outbreak rather than isolated imported cases. For official NPI
218 dates see Table 1.

220 **SEIR model.** We model SARS-CoV-2 infection dynamics by following the number of susceptible S , exposed
 E , reported infected I_r , unreported infected I_u , and recovered R individuals in a population of size N . This
model distinguishes between reported and unreported infected individuals: the reported infected are those that
222 have enough symptoms to eventually be tested and thus appear in daily case reports, to which we fit the model.
This model is inspired by Li et al.¹⁷ and Pei and Shaman¹⁸, who used a similar model with multiple regions

*Sweden banned public events on Mar 12, encouraged social distancing on Mar 16, and closed schools on Mar 18⁹.

224 and constant transmission and reporting rates to study COVID-19 dynamics in China and in the continental
 US.
 226 Susceptible (S) individuals become exposed due to contact with reported or unreported infected individuals (I_r
 or I_u) at a rate β_t or $\mu\beta_t$, respectively. The parameter $0 < \mu < 1$ represents the decreased transmission rate
 228 from unreported infected individuals, who are often subclinical or even asymptomatic^{8,20}. The transmission
 rate $\beta_t \geq 0$ may change over time t due to behavioural changes of both susceptible and infected individuals.
 230 Exposed individuals, after an average latent period of Z days, become reported infected with probability α_t or
 unreported infected with probability $(1 - \alpha_t)$. The reporting rate $0 < \alpha_t < 1$ may also change over time due
 232 to changes in human behaviour. Infected individuals remain infectious for an average period of D days, after
 which they either recover, or become ill enough to be quarantined. In either case, they no longer infect other
 234 individuals, and therefore effectively become recovered (R). The model is described by the following set of
 equations,

$$\begin{aligned} \frac{dS}{dt} &= -\beta_t S \left(\frac{I_r}{N} + \mu \frac{I_u}{N} \right) \\ \frac{dE}{dt} &= \beta_t S \left(\frac{I_r}{N} + \mu \frac{I_u}{N} \right) - \frac{E}{Z} \\ \frac{dI_r}{dt} &= \alpha_t \frac{E}{Z} - \frac{I_r}{D} \\ \frac{dI_u}{dt} &= (1 - \alpha_t) \frac{E}{Z} - \frac{I_u}{D} \\ \frac{dR}{dt} &= \frac{I_r}{D} + \frac{I_u}{D}, \end{aligned} \tag{1}$$

236 where N is the population size. The initial numbers of exposed $E(0)$ and unreported infected $I_u(0)$ are free
 238 model parameters (i.e. inferred from the data), whereas the initial number of reported infected and recovered is
 assumed to be zero, $I_r(0) = R(0) = 0$, and the number of susceptible is $S(0) = N - E(0) - I_u(0)$.

240 **Likelihood function.** For a given vector θ of model parameters the *expected* cumulative number of reported
 infected individuals (I_r) until day t , following Eq. 1, is

$$242 \quad Y_t(\theta) = \int_0^t \alpha_s \frac{E(s)}{Z} ds, \quad Y_0 = 0. \tag{2}$$

244 We assume that reported infected individuals are confirmed and therefore observed in the daily case report of
 day t with probability p_t (note that an individual can only be observed once, and that p_t may change over time,
 but t is a specific date rather than the time elapsed since the individual was infected). We denote by X_t the
 246 *observed* number of confirmed cases in day t , and by \tilde{X}_t the cumulative number of confirmed cases until end of
 day t ,

$$248 \quad \tilde{X}_t = \sum_{i=1}^t X_i. \tag{3}$$

Therefore, at day t the number of reported infected yet-to-be confirmed individuals is $(Y_t(\theta) - \tilde{X}_{t-1})$. We assume
 250 that X_t conditioned on \tilde{X}_{t-1} is Poisson distributed, such that

$$\begin{aligned} (X_1 | \theta) &\sim Poi(Y_1(\theta) \cdot p_1), \\ (X_t | \tilde{X}_{t-1}, \theta) &\sim Poi((Y_t(\theta) - \tilde{X}_{t-1}) \cdot p_t), \quad t = 2, \dots, T. \end{aligned} \tag{4}$$

252 Hence, the *likelihood function* $\mathcal{L}(\theta | \mathbf{X})$ for a parameter vector θ given the confirmed case data $\mathbf{X} = (X_1, \dots, X_T)$
 is defined by the probability to observe \mathbf{X} given θ ,

$$254 \quad \mathcal{L}(\theta | \mathbf{X}) = P(\mathbf{X} | \theta) = P(X_1 | \theta) \cdot P(X_2 | \tilde{X}_1, \theta) \cdots P(X_T | \tilde{X}_{T-1}, \theta). \tag{5}$$

NPI model. To model non-pharmaceutical interventions (NPIs), we set the start of the NPIs to day τ and define

$$\beta_t = \begin{cases} \beta, & t < \tau \\ \beta\lambda, & t \geq \tau \end{cases}, \quad \alpha_t = \begin{cases} \alpha_1, & t < \tau \\ \alpha_2, & t \geq \tau \end{cases}, \quad p_t = \begin{cases} 1/9, & t < \tau \\ 1/6, & t \geq \tau \end{cases}, \quad (6)$$

where $0 < \lambda < 1$. The values for p_t follow Li et al.¹⁷, who estimated the average time between infection and reporting in Wuhan, China, at 9 days before the start of NPIs and 6 days after start of NPIs.

Following Li et al.¹⁷, the effective reproduction numbers before and after the start of NPIs are

$$\begin{aligned} R_1 &= \alpha_1\beta D + (1 - \alpha_1)\mu\beta D, \\ R_2 &= \alpha_2\lambda\beta D + (1 - \alpha_2)\mu\lambda\beta D. \end{aligned} \quad (7)$$

The relative reduction in the effective reproduction number due to NPIs is $\frac{R_1 - R_2}{R_1}$.

Parameter estimation. To estimate the model parameters from the daily case data \mathbf{X} , we apply a Bayesian inference approach. Model fitting was calibrated for case data up to Mar 28, and then applied to data up to Apr 11 (for Wuhan, China, model fitting was applied for data up to Feb 8.) We start our model Δt days¹¹ before the outbreak (defined as consecutive days with increasing confirmed cases) in each country. The model in Eqs. 1 and 6 is parameterised by the vector θ , where

$$\theta = (Z, D, \mu, \beta, \lambda, \alpha_1, \alpha_2, E(0), I_u(0), \Delta t, \tau). \quad (8)$$

The likelihood function is defined in Eq. 5. We defined the following prior distributions on the model parameters $P(\theta)$:

$$\begin{aligned} Z &\sim Uniform(2, 5) \\ D &\sim Uniform(2, 5) \\ \mu &\sim Uniform(0.2, 1) \\ \beta &\sim Uniform(0.8, 1.5) \\ \lambda &\sim Uniform(0, 1) \\ \alpha_1, \alpha_2 &\sim Uniform(0.02, 1) \\ E(0) &\sim Uniform(0, 3000) \\ I_u(0) &\sim Uniform(0, 3000) \\ \Delta t &\sim Uniform(1, 5) \\ \tau &\sim TruncatedNormal\left(\frac{\tau^* + \tau^0}{2}, \frac{\tau^* - \tau^0}{2}, 5, T - 2\right), \end{aligned} \quad (9)$$

where the prior for τ is a truncated normal distribution shaped so that the date of the first and last NPI, τ^0 and τ^* (Table 1), are at minus and plus one standard deviation, and taking values only between 5 and $T - 2$, where T is the number of days in the data \mathbf{X} . We also tested an uninformative uniform prior, $Uniform(1, T - 2)$. WAIC (Eq. 10) of a model with this uniform prior was either higher, or lower by less than 2, compared to WAIC of a model with the truncated normal prior. The uninformative prior resulted in non-negligible posterior probability for unreasonable τ values, such as Mar 1 in the United Kingdom. We therefore decided to use the more informative truncated normal prior for τ . Other priors follow Li et al.¹⁷, with the following exceptions. λ is used to ensure transmission rates are lower after the start of the NPIs ($\lambda < 1$). We checked values of Δt larger than five days and found they generally produce lower likelihood and unreasonable parameter estimates, and therefore chose $Uniform(1, 5)$ as the prior for Δt . We also tried to estimate the value of p_t before and after τ , instead of keeping it fixed at 1/9 and 1/6. The model with fixed values was supported by the evidence (lower WAIC, see below) in 9 of 12 countries. Moreover, the estimates for Wuhan, China were 1/9 and 1/6, as in Li et al.¹⁷.

The posterior distribution of the model parameters $P(\theta | \mathbf{X})$ is estimated using the affine-invariant ensemble sampler for Markov chain Monte Carlo (MCMC)¹³, implemented in the emcee Python package¹⁰. We use

the default configuration using the stretch move with stretch scale parameter $a = 2$. For the main analysis we
 288 use 50 chains (or walkers) per region, with 7M samples per chain (no thinning was applied). The *integrated*
autocorrelation time (IAT)^{10,13} was averaged across parameters and chains for each region. The IAT was
 290 between 32K for Wuhan, China, and 187K for Germany (Figure S6). We examined the trace plots for τ in all
 292 regions (Figure S7). All chains seem to converge to the same stationary distribution, in most cases before 2M
 294 steps. Thus, we discarded the first 2M samples as burn-in samples. The only exception is Spain, in which a
 296 single chain converged at around 6M steps. We considered this chain as part of the burn-in and removed it
 298 from the analysis. Therefore, 50 chains with 5M samples and IAT between 40K and 187K give an effective
 samples size between 1,335 and 7,812. We ran additional chains with 2M samples and a different initialization
 (i.e. seed). The estimated posterior distributions of τ were very similar to our main analysis, further increasing
 our confidence in the convergence of our inference. We also examined the joint posterior distributions of τ and
 λ (Figure S4).

Model comparison. We perform model selection using two methods. First, we compute WAIC (widely
 300 applicable information criterion)¹²,

$$WAIC(\theta | \mathbf{X}) = -2 \log \mathbb{E}[\mathcal{L}(\theta | \mathbf{X})] + 2\mathbb{V}[\log \mathcal{L}(\theta | \mathbf{X})] \quad (10)$$

302 where $\mathbb{E}[\cdot]$ and $\mathbb{V}[\cdot]$ are the expectation and variance operators taken over the posterior distribution $P(\theta | \mathbf{X})$.
 We compare models by reporting their relative WAIC; lower is better (Table S1).

304 We also plot posterior predictions: we sample 1,000 parameter vectors from the posterior distribution $P(\theta | \mathbf{X})$
 fitted to data up to Apr 11, use these parameter vectors to simulate the SEIR model (Eq. 1) up to Apr 24, and plot
 306 the predicted dynamics (Figure S3). Both the accuracy (i.e. overlap of data and prediction) and the precision
 (i.e. the tightness of the predictions) are good ways to visually compare models. We also compute the expected
 308 posterior RMSE (root mean squared error) of these predictions (Table S2).

Declarations

310 **Ethics approval and consent to participate.** Not applicable.

Consent for publication. Not applicable.

312 **Availability of data and materials.** We use Python 3 with NumPy, Matplotlib, SciPy, Pandas, Seaborn, and
 emcee. Source code will be publicly available under a permissive open-source license at github.com/yoavram-lab/EffectiveNPI. We used freely available data, see source code repository and above *Data* section for details.

316 **Competing interests.** The authors declare that they have no competing interests.

Funding. This work was supported in part by the Israel Science Foundation (3811/19 and 552/19, YR). The
 318 funding body had no role in designing, performing, or analyzing the study.

Authors' contributions. UO and YR designed the research. IK and YR performed the research and wrote the
 320 manuscript. All authors read and approved the final manuscript.

Acknowledgements. We thank Yinon M. Bar-On, Lilach Hadany, Oren Kolodny, and Zohar Yakhini.

Region	τ^*	$\hat{\tau}$	$HDI_{75\%}$	$HDI_{95\%}$	Z	D	μ	β	α_1	λ	α_2	$E(0)$	$I_u(0)$	Δt		
Austria	Mar 16	Mar 21	-2.8240	2.5130	-4.2967	3.5110	3.9362	0.63066	0.1468	0.1592	0.1370	0.2667	128.6634	111.2741	2.2407	
Belgium	Mar 18	Mar 27	-1.5528	2.3908	-3.4283	2.3908	4.0266	3.6358	0.5031	0.0780	0.2536	0.4572	0.1927	327.7634	417.8771	2.1455
Denmark	Mar 18	Mar 11	-5.3104	2.5859	-7.4123	15.7701	4.0140	3.4301	0.4149	0.0594	0.1546	0.6977	0.2041	268.2553	370.4863	2.2678
France	Mar 17	Mar 24	-0.4310	0.5557	-1.4388	2.6488	4.2107	3.0919	0.4713	1.0555	0.3823	0.3789	0.4142	412.7334	1324.2711	1.6487
Germany	Mar 22	Mar 19	-0.5544	0.9207	-0.9874	0.9205	3.3868	3.6944	0.6963	1.1670	0.1464	0.2735	0.3464	555.4142	512.6100	2.1134
Italy	Mar 11	Mar 17	-0.9537	2.4978	-2.0064	3.0463	4.1810	2.6012	0.5307	0.9845	0.5554	0.3819	0.4918	1046.1239	1934.9495	1.6776
Norway	Mar 24	Mar 22	-3.9815	4.5891	-12.0256	5.5891	4.0587	3.1077	0.3949	1.0343	0.1564	0.3105	0.2447	471.9163	828.4834	2.0465
Spain	Mar 14	Mar 25	-0.7436	0.6951	-1.4311	1.6951	4.0898	3.2785	0.5791	1.1420	0.3861	0.2521	0.3091	263.3634	866.9249	1.6239
Sweden	Mar 18	Mar 09	-4.9651	4.0108	-6.9652	11.2502	4.0167	3.3536	0.3691	1.0414	0.1304	0.7359	0.3024	398.0938	541.5147	2.4724
Switzerland	Mar 20	Mar 19	-1.5556	1.2313	-1.7802	3.1982	3.9322	3.5641	0.6174	1.1477	0.1617	0.2452	0.2787	277.1029	312.9546	2.0510
United Kingdom	Mar 24	Mar 26	-1.4515	1.2782	-2.1466	2.2780	3.9944	3.4811	0.6180	1.1208	0.1959	0.4468	0.2597	288.9485	330.3028	2.0867
Wuhan, China	Jan 23	Feb 02	-1.4380	2.0284	-2.9716	2.2892	3.7473	3.6828	0.6026	1.1391	0.2805	0.1825	0.3511	610.6800	544.0883	2.3823

Table 2: Parameter estimates for different regions. See Eq. 1 for model parameters. All estimates are posterior medians. 75% and 95% credible intervals (HDI) are given for τ in days relative to $\hat{\tau}$. τ^* is the official last NPI date (Table 1).

322 **References**

- [1] Ali, S. T., Wang, L., Lau, E. H. Y., Xu, X.-K., Du, Z., Wu, Y., Leung, G. M. and Cowling, B. J. 2020, ‘Serial interval of SARS-CoV-2 was shortened over time by nonpharmaceutical interventions’, *Science* (80-.). **9004**(July), eabc9004.
- [2] Arthur, R. F., Jones, J. H., Bonds, M. H. and Feldman, M. W. 2020, ‘Complex dynamics induced by delayed adaptive behavior during outbreaks’, *bioRxiv* pp. 1–23.
- [3] Atchison, C. J., Bowman, L., Vrinten, C., Redd, R., Pristera, P., Eaton, J. W. and Ward, H. 2020, ‘Perceptions and behavioural responses of the general public during the COVID-19 pandemic: A cross-sectional survey of UK Adults’, *medRxiv* p. 2020.04.01.20050039.
- [4] Banholzer, N., Weenen, E. V., Kratzwald, B. and Seeliger, A. 2020, ‘The estimated impact of non-pharmaceutical interventions on documented cases of COVID-19 : A cross-country analysis’, *medRxiv*.
- [5] Bar-On, Y. M., Flamholz, A., Phillips, R. and Milo, R. 2020, ‘SARS-CoV-2 (COVID-19) by the numbers’, *Elife* **9**.
- [6] Dunn, A. G., Leask, J., Zhou, X., Mandl, K. D. and Coiera, E. 2015, ‘Associations between exposure to and expression of negative opinions about human papillomavirus vaccines on social media: An observational study’, *J. Med. Internet Res.* **17**(6), e144.
- [7] Fenichel, E. P., Castillo-Chavez, C., Ceddia, M. G., Chowell, G., Gonzalez Parrae, P. A., Hickling, G. J., Holloway, G., Horan, R., Morin, B., Perrings, C., Springborn, M., Velazquez, L. and Villalobos, C. 2011, ‘Adaptive human behavior in epidemiological models’, *Proc. Natl. Acad. Sci. U. S. A.* **108**(15), 6306–6311.
- [8] Ferretti, L., Wymant, C., Kendall, M., Zhao, L., Nurtay, A., Abeler-Dörner, L., Parker, M., Bonsall, D. and Fraser, C. 2020, ‘Quantifying SARS-CoV-2 transmission suggests epidemic control with digital contact tracing’, *Science* (80-.). **368**(6491), eabb6936.
- [9] Flaxman, S., Mishra, S., Gandy, A., Unwin, H. J. T., Mellan, T. A., Coupland, H., Whittaker, C., Zhu, H., Berah, T., Eaton, J. W., Monod, M., Ghani, A. C., Donnelly, C. A., Riley, S. M., Vollmer, M. A. C., Ferguson, N. M., Okell, L. C. and Bhatt, S. 2020, ‘Estimating the effects of non-pharmaceutical interventions on COVID-19 in Europe’, *Nature* (March), 1–35.
- [10] Foreman-Mackey, D., Hogg, D. W., Lang, D. and Goodman, J. 2013, ‘emcee : The MCMC Hammer’, *Publ. Astron. Soc. Pacific* **125**(925), 306–312.
- [11] Gatto, M., Bertuzzo, E., Mari, L., Miccoli, S., Carraro, L., Casagrandi, R. and Rinaldo, A. 2020, ‘Spread and dynamics of the COVID-19 epidemic in Italy: Effects of emergency containment measures’, *Proc. Natl. Acad. Sci. U. S. A.* p. 202004978.
- [12] Gelman, A., Carlin, J. B., Stern, H. S., Dunson, D. B., Vehtari, A. and Rubin, D. B. 2013, *Bayesian Data Analysis, Third Edition*, Chapman & Hall/CRC Texts in Statistical Science, Taylor & Francis.
- [13] Goodman, J. and Weare, J. 2010, ‘Ensemble Samplers With Affine Invariance’, *Commun. Appl. Math. Comput. Sci.* **5**(1), 65–80.
- [14] Kass, R. E. and Raftery, A. E. 1995, ‘Bayes Factors’, *J. Am. Stat. Assoc.* **90**(430), 773.
- [15] Kaufman, M. R., Cornish, F., Zimmerman, R. S. and Johnson, B. T. 2014, ‘Health behavior change models for HIV prevention and AIDS care: Practical recommendations for a multi-level approach’, *J. Acquir. Immune Defic. Syndr.* **66**(SUPPL.3), 250–258.

- [16] Kruschke, J. K. 2015, *Doing Bayesian Data Analysis A Tutorial with R, JAGS, and Stan*, Academic Press.
- [17] Li, R., Pei, S., Chen, B., Song, Y., Zhang, T., Yang, W. and Shaman, J. 2020, ‘Substantial undocumented infection facilitates the rapid dissemination of novel coronavirus (SARS-CoV2)’, *Science* (80-). p. eabb3221.
- [18] Pei, S. and Shaman, J. 2020, ‘Initial Simulation of SARS-CoV2 Spread and Intervention Effects in the Continental US’, *medRxiv* p. 2020.03.21.20040303.
- [19] Smith, L. E., Mottershaw, A. L., Egan, M., Waller, J., Marteau, T. M. and Rubin, G. J. 2020, ‘The impact of believing you have had COVID-19 on behaviour : Cross-sectional survey’, *medRxiv* pp. 1–20.
- [20] Thompson, R. N., Lovell-Read, F. A. and Obolski, U. 2020, ‘Time from Symptom Onset to Hospitalisation of Coronavirus Disease 2019 (COVID-19) Cases: Implications for the Proportion of Transmissions from Infectors with Few Symptoms’, *J. Clin. Med.* **9**(5), 1297.
- [21] Walters, C. E. and Kendal, J. R. 2013, ‘An SIS model for cultural trait transmission with conformity bias’, *Theor. Popul. Biol.* **90**, 56–63.
- [22] Wiyeh, A. B., Cooper, S., Nnaji, C. A. and Wiysonge, C. S. 2018, ‘Vaccine hesitancy ’outbreaks’: using epidemiological modeling of the spread of ideas to understand the effects of vaccine related events on vaccine hesitancy’, *Expert Rev. Vaccines* **17**(12), 1063–1070.
- [23] Zipfel, C. M. and Bansal, S. 2020, ‘Assessing the interactions between COVID-19 and influenza in the United States’, *medRxiv* (February), 1–13.

Supplementary Material

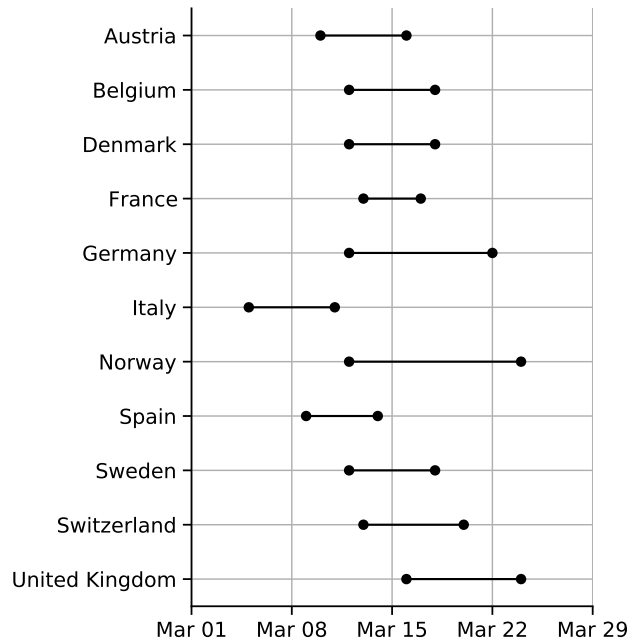


Figure S1: Official start of non-pharmaceutical interventions. See Table 1 for more details. Wuhan, China is not shown.

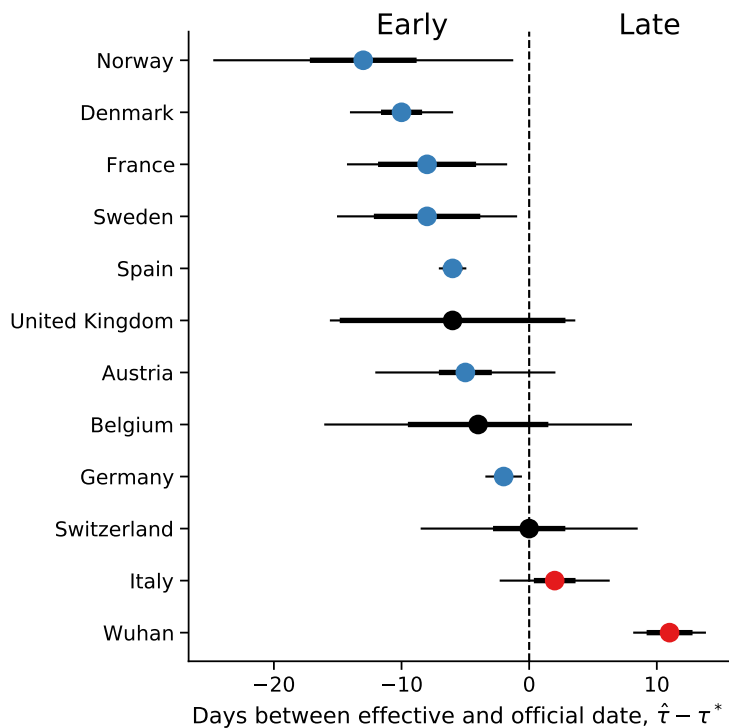


Figure S2: Official vs. effective start of non-pharmaceutical interventions estimated up to Mar 28. The difference between τ the effective and τ^* the official start of NPIs estimated from case data up to Mar 28, 2020, shown for different regions. Here, $\hat{\tau}$ is the marginal posterior median. τ^* is the last NPI date (a lockdown everywhere by Sweden, see Table 1). Thin and bold lines show 95% and 75% credible intervals (HDI¹⁶), respectively. Inference performed similarly to main inference, but with data up to Mar 28 and only 1M samples per chain with 600K burn-in.

WAIC

Country	No	Fixed	Free
Austria	219.49	95.06	35.96
Belgium	148.37	98.41	49.16
Denmark	44.36	40.30	43.11
France	581.59	255.14	172.08
Germany	1029.36	327.50	174.90
Italy	898452.34	5484.56	80.18
Norway	70.03	42.04	39.79
Spain	1476.46	647.34	128.58
Sweden	32.53	30.06	31.10
Switzerland	265.80	83.95	63.89
United Kingdom	258.18	117.54	68.17
Wuhan China	107.31	94.00	73.75

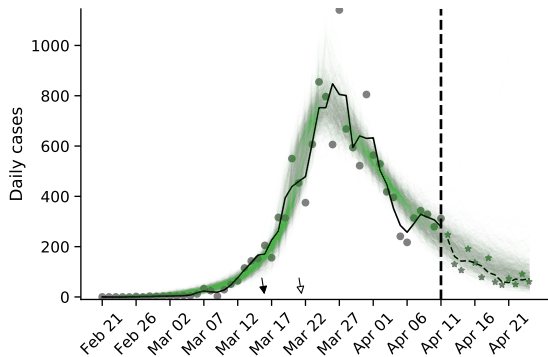
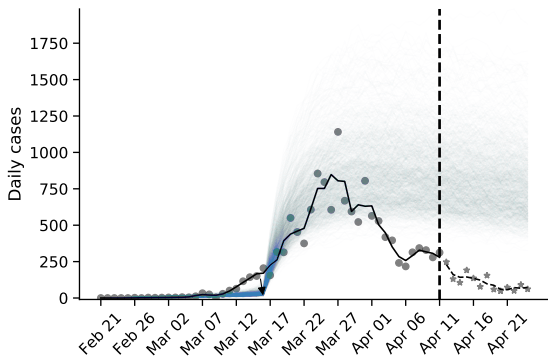
Table S1: WAIC values for the different models. WAIC (widely applicable information criterion; Eq. 10)¹² values for models with: no τ at all, *No*; τ fixed at the official last NPI date τ^* , *Fixed*; and free parameter τ , *Free*. WAIC values are scaled as a deviance measure: lower values imply higher predictive accuracy and a difference of 2 is a popular threshold for model comparison¹⁴. Bold values emphasize cases in which the *Free* model has the lowest WAIC.

RMSE

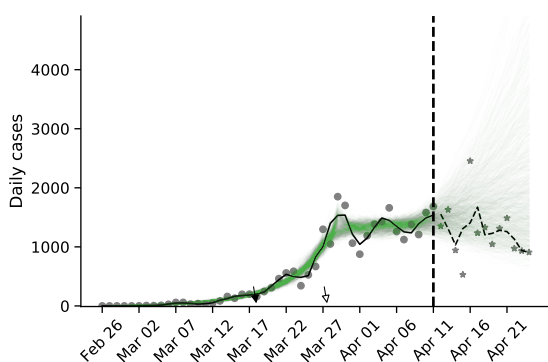
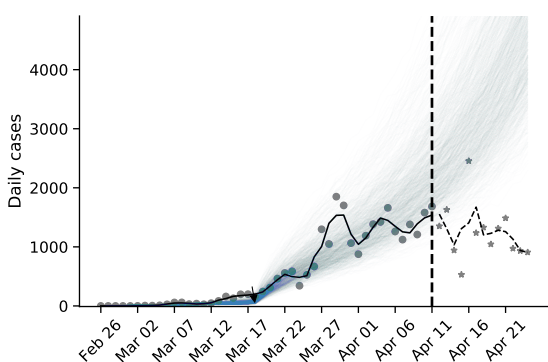
Country	No	Fixed	Free
Austria	926.7	740.7	58.9
Belgium	3286.0	2541.0	902.9
Denmark	434.8	1058.0	400.0
France	10530.0	8206.0	1816.0
Germany	14240.0	17760.0	1952.0
Italy	14160.0	9536.0	1106.0
Norway	292.2	578.2	63.3
Spain	17840.0	14410.0	1704.0
Sweden	775.9	1205.0	596.4
Switzerland	1839.0	1721.0	214.0
United Kingdom	14700.0	14780.0	2735.0

Table S2: Posterior RMSE of out-of-sample predictions with the different models. Expected posterior predictive RMSE (root mean squared error) for models with: no τ at all, *No*; τ fixed at the official last NPI date τ^* , *Fixed*; and free parameter τ , *Free*. In all cases, the model with free parameter τ has the lowest RMSE. Models were fitted to case data up to Apr 11, 2020, and then used to generate 1,000 predictions up to Apr 24 by sampling model parameters from the posterior distribution. These predictions were then compared to the real data using RMSE, and the mean RMSE value is shown in the table for each country and model. Bold values emphasize cases in which the *Free* model has the lowest RMSE.

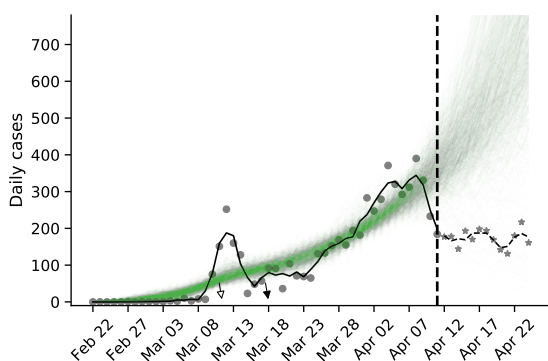
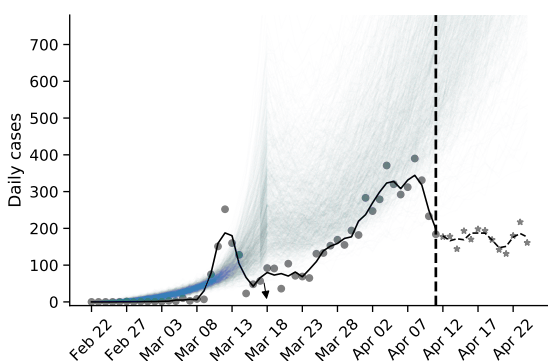
Austria



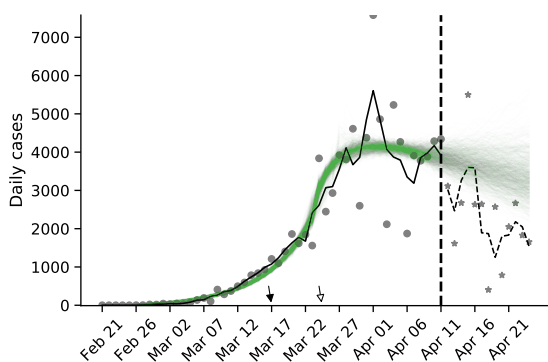
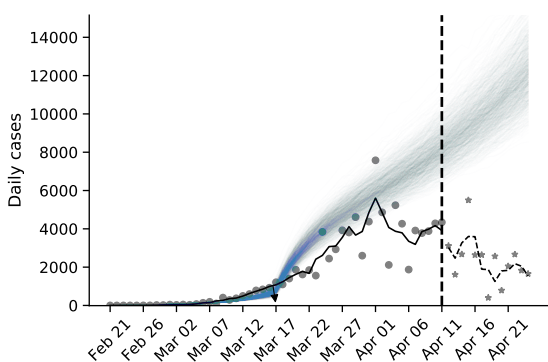
Belgium



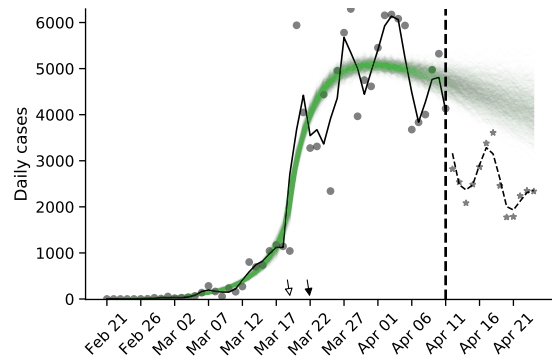
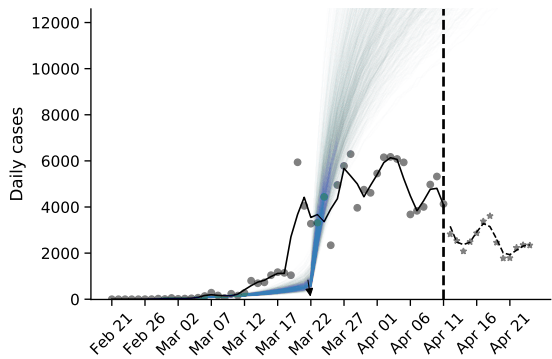
Denmark



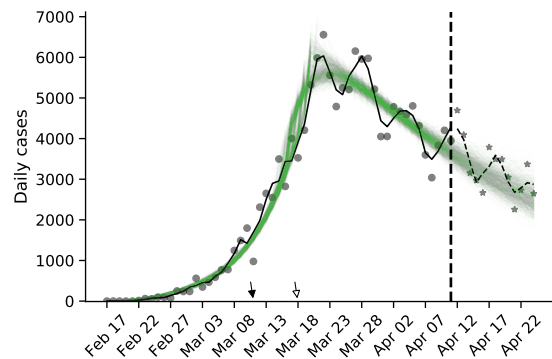
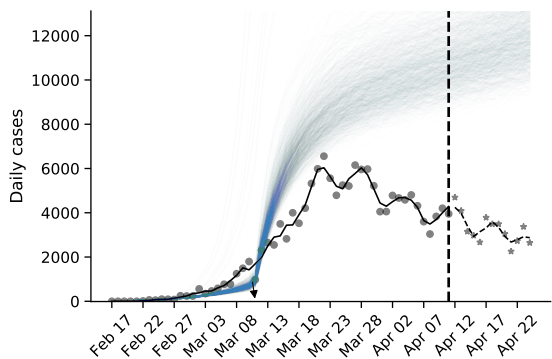
France



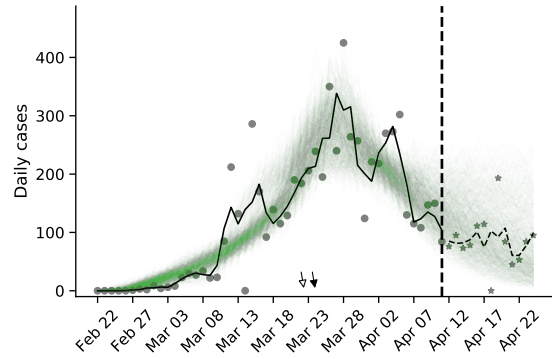
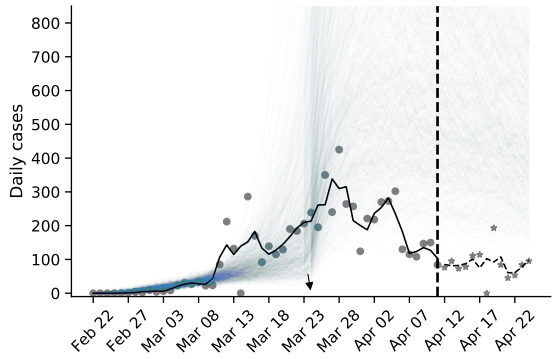
Germany



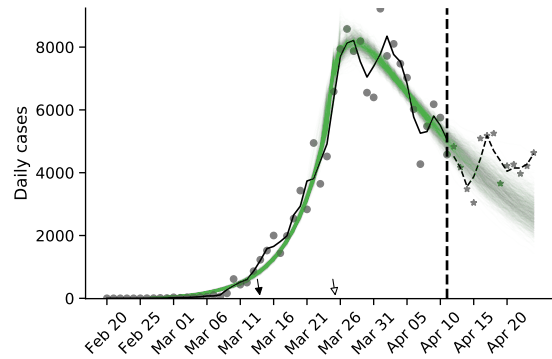
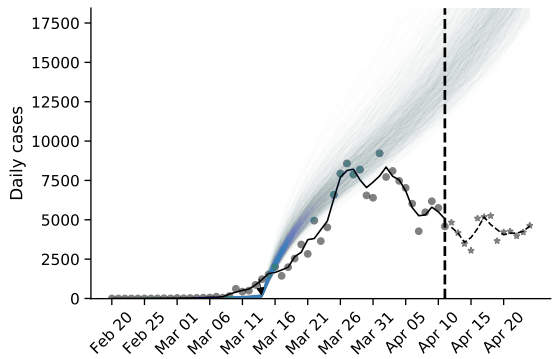
Italy



Norway



Spain



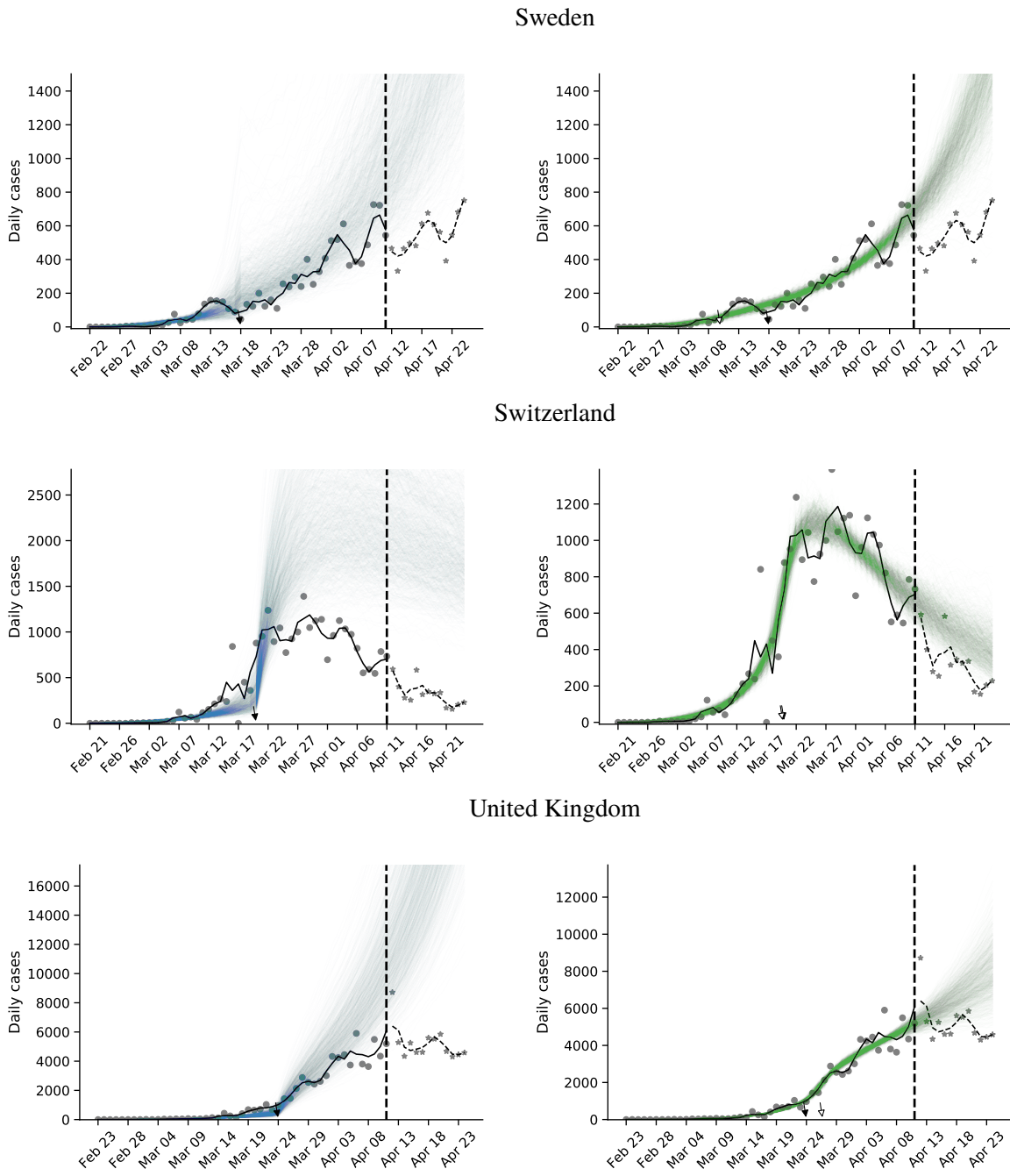


Figure S3: Posterior prediction plots for 11 European countries. The vertical dashed line represents Apr 11, 2020. Circles and stars represent daily case data up to and after Apr 11, respectively. Black and white arrows denote the official τ^* and effective $\hat{\tau}$ start of NPIs, respectively. Black lines represent a smoothing of the data points using a Savitzky-Golay filter with window length 3. Coloured lines represent posterior predictions from a model with fixed τ (blue) and free τ (green). Models were fitted with data up to Apr 11. The predictions are generated by drawing 1,000 parameter sets from the posterior distribution, and then generating a daily case count using the SEIR model (Eq. 1) up to Apr 24. Note the differences in the y-axis scale. Posterior predictions with the free τ model predict the out-of-sample data well for all countries except Denmark and Sweden, but poorly with the fixed τ model. The predictions of the model without τ (not shown) are even worse.

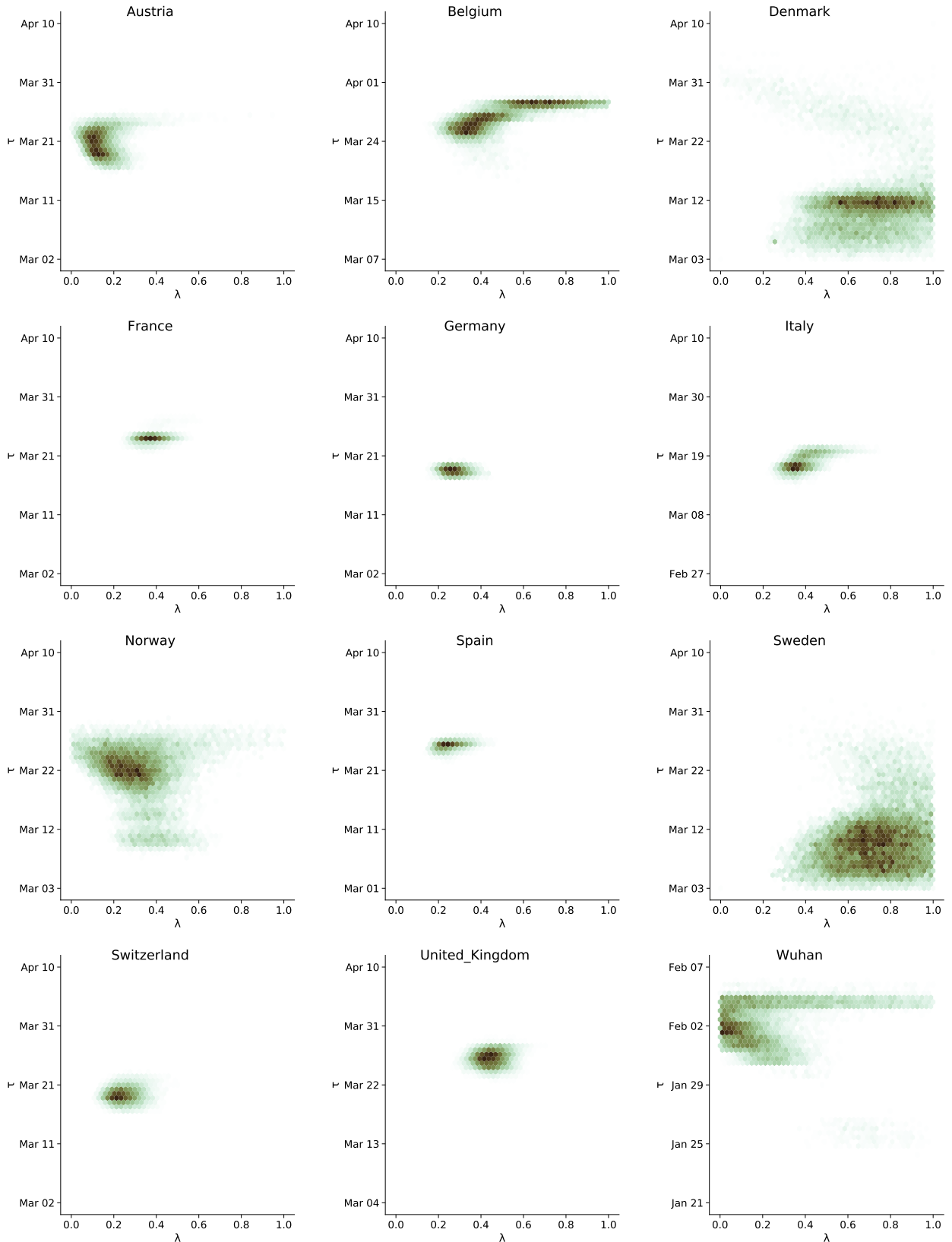


Figure S4: Joint posterior density plots for τ and λ . The high values of λ estimated in Denmark and Sweden reduce the effect of the NPIs thereby making the inference of τ more difficult, resulting in wide posterior distributions. A correlation between the parameters is also evident in Norway. In Belgium and in Wuhan a later τ gives a wide estimate for λ . In comparison, Austria, France, Germany, Italy, Spain, Switzerland, and UK have a narrow joint distribution.

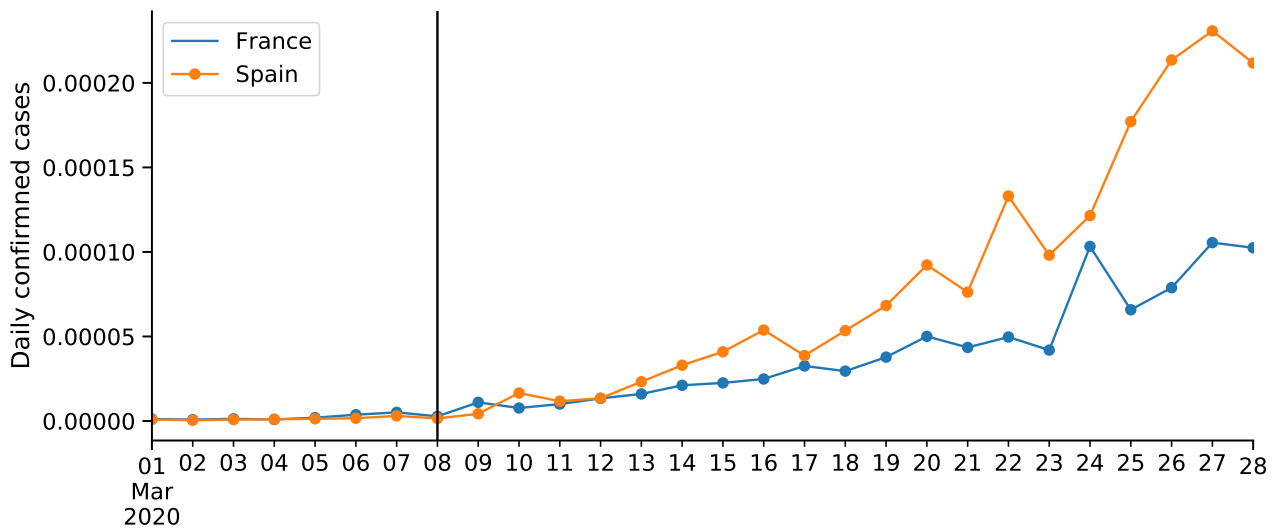


Figure S5: COVID-19 daily confirmed cases in France and Spain. Number of cases proportional to population size (as of 2018). Vertical line shows Mar 8, the effective start of NPIs $\hat{\tau}$ in both countries. Data from Flaxman et al.⁹.

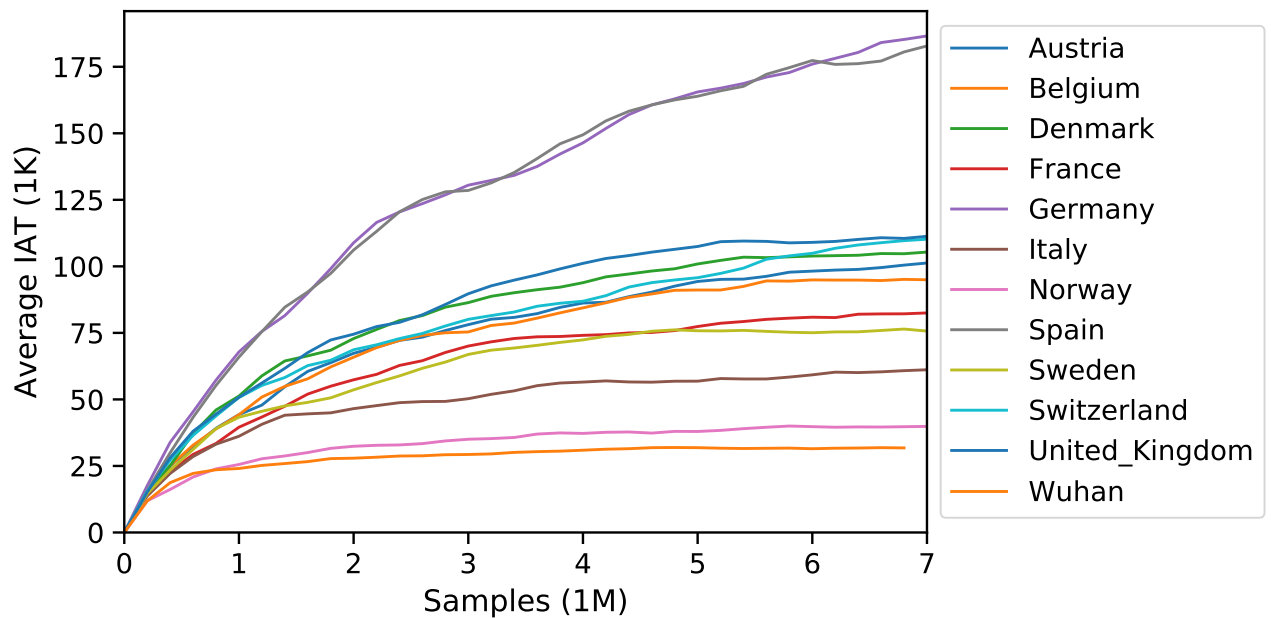


Figure S6: Integrated autocorrelation time (IAT)^{10,13}, averaged across model parameters and MCMC chains, as a function of the number of samples in the chains. IAT is less than 187K in all cases, while chain length is 5M after burn-in period of 2M. With 50 chains per region, this gives a at least 1,335 uncorrelated samples for estimating the posterior distribution.

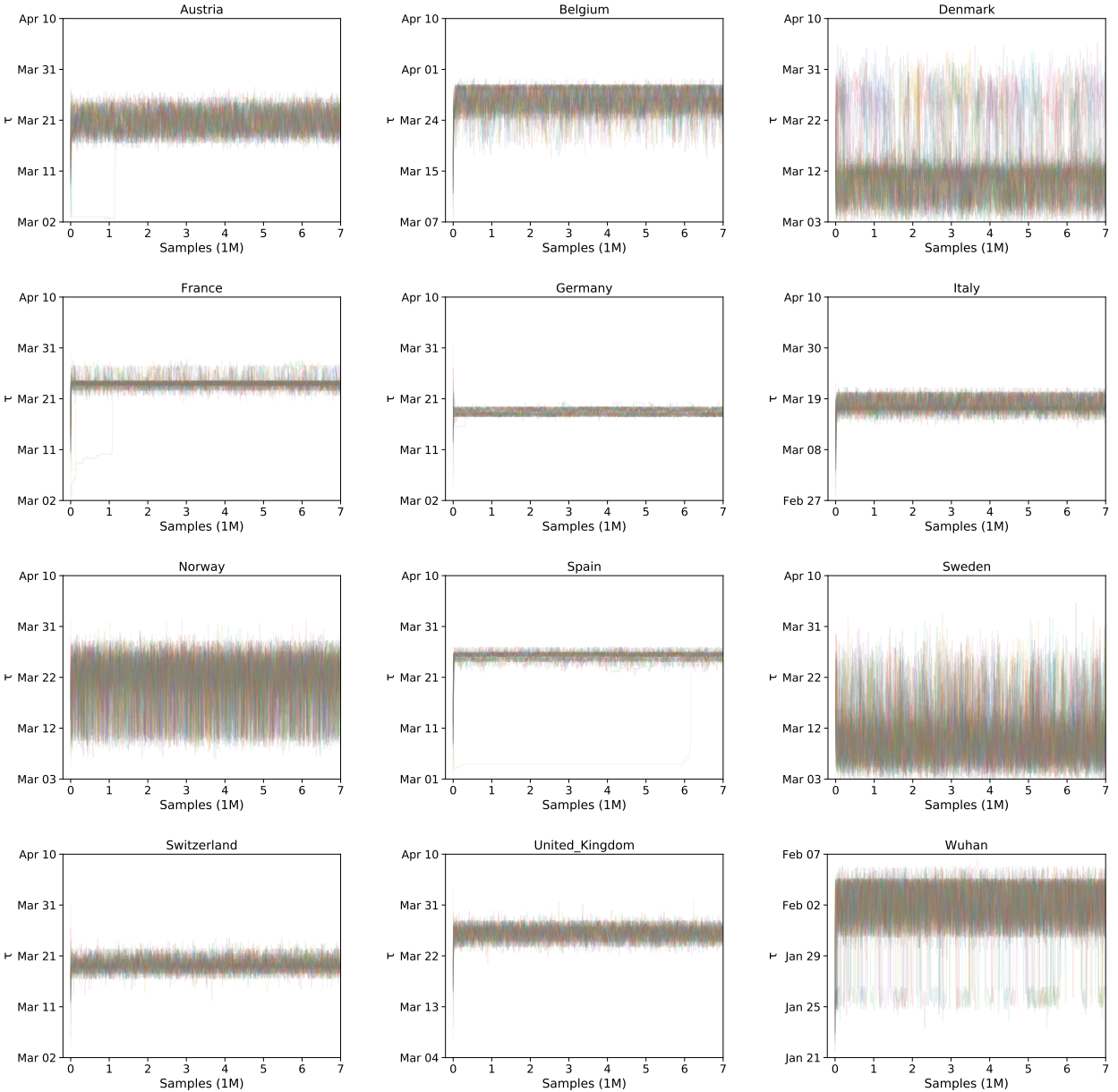


Figure S7: Trace plots for τ . The value of τ at for sequential samples of 50 chains per region. To facilitate visualization, chains were thinned 1:10,000 for the trace plots, but not for posterior estimation. Line transparency was set at $\alpha = 0.1$ and chains cycle through different colors. In France and Austria some chains converged relatively late but before the burn-in period (2M iterations). In Spain, a single chain converged very late (after roughly 6M iterations) and was removed from further analysis. The y-axis range is the support of the prior on τ .